A Sensitivity Model for Predicting Photonic Crystal Biosensor Performance

Ian D. Block, Nikhil Ganesh, Meng Lu, and Brian T. Cunningham, *Senior Member, IEEE*

***Abstract*—We present a model for predicting photonic crystal label-free biosensor performance based primarily on the spatial distribution of electromagnetic near fields at device resonance. To achieve maximum device sensitivity, the resonant fields can be shaped by careful choice of material and geometrical parameters. The effect of each property on the resonant mode profile, and consequently on sensor performance, is illustrated. A comparison of device sensitivity calculated by both the proposed model and direct rigorous coupled wave analysis simulation supports the validity of our model.**

***Index Terms*—Biomedical transducers, optical resonance.**

I. Introduction

LABEL-FREE photonic-based bionsensors have gained much attention recently for their high sensitivity and utility for detecting biomolecular interactions [1]. Normal-incidence white-light illumination, simple readout instrumentation, high spatial resolution imaging, and inexpensive replication-based fabrication approaches have contributed to the utilization of photonic crystal (PC) biosensors for a wide range of applications in pharmaceutical discovery and life science research [2]. Recent experimental results have shown that modification of the refractive index of the periodic surface structure and scaling of the PC periodicity have both lead to improved sensor performance [3], [4]. We present here a theoretical basis for these findings and use rigorous coupled wave analysis (RCWA) to visualize how the resonant fields interact with biological media. Furthermore, we stress the fundamental differences between surface sensitivity, which is useful in the context of detecting thin layers of adsorbed biomolecules, and bulk sensitivity which is correlated with detecting larger objects like cells or refractive index fluctuations of the test media.

The biosensor structure, shown schematically in Fig. 1, is a one-dimensional surface PC comprised of a low refractive index linear grating surface structure coated with a high refractive index film. For such a subwavelength structure, the zeroth diffracted orders propagate, while all higher orders are cutoff. Upon illumination with polarized white light at normal incidence, the evanescent ± 1 diffracted orders couple to counter-propagating leaky waves that form a standing wave within the periodically modulated layer [5]. Phase matching by the periodic structure to the reflected and transmitted zeroth orders enables rapid extraction of energy from the leaky waves [6], [7]. Constructive interference of the outcoupled light with the backward diffracted zeroth order and destructive interference with the forward diffracted zeroth order yields a sharp resonant reflection peak with 100% efficiency [8].

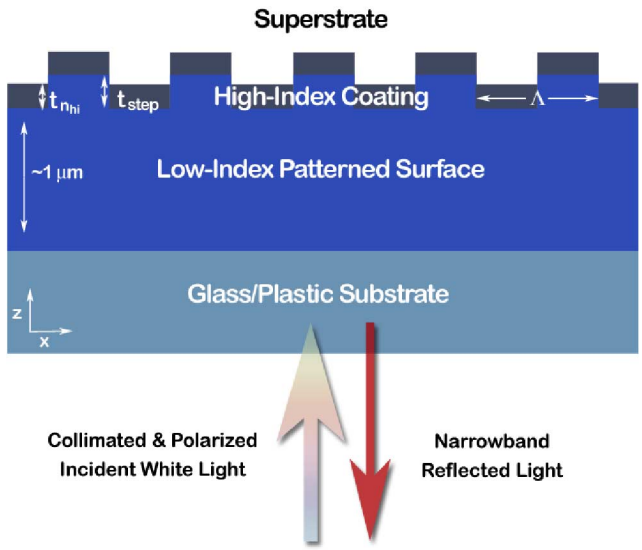

Fig. 1. Photonic crystal biosensor schematic. Period (Λ), high index coating thickness (t_{hi}), and grating step height (t_{step}).

The design of label-free PC-based biosensors requires knowledge of how the material and structural properties of the device ultimately dictate biosensor performance. While the relationship between physical sensor properties and the characteristics of the reflection spectra has been previously characterized, we focus here on the relationship between the resonant mode electric field distribution and its impact on biosensor sensitivity. Consideration of the electric field interaction with adsorbed layers of biomaterial is used to guide optimization of the photonic crystal structural and material parameters.

II. Sensitivity Quantification

Like all optical resonators, the PC employed in this work stores energy at resonance. This energy is manifested as optical near fields that interact with the device itself as well as with the external environment. Energy is injected into and extracted from the resonant standing waves through phase matching provided by the periodic modulation, as discussed in the previous section. Changes of the external environment lead to modified

Manuscript received September 10, 2007; revised November 11, 2007; accepted November 8, 2007. This work was supported in part by the National Science Foundation under Grant BES 04-27657 and in part by SRU Biosystems. The associate editor coordinating the review of this paper and approving it for publication was Dr. Andreas Hierlemann.

The authors are with the University of Illinois Urbana–Champaign, Urbana, IL 61801 USA (e-mail: iblock2@uiuc.edu; nganesh2@uiuc.edu; menglv@uiuc.edu; bcunning@uiuc.edu).

Color versions of one or more of the figures in this paper are available online at http://ieeexplore.ieee.org.

Digital Object Identifier 10.1109/JSEN.2008.917127

near fields and concomitant spectral changes of the reflected far fields which are easily measured. In order to understand how the spectral response varies with the sensor design and to maximize the spectral tuning due to changes of the sensor's environment, we develop here a model that equates device geometry and material parameters to the resulting sensor response. For normal incidence illumination, the response of the photonic crystal is coupled to the second-order Bragg condition and, therefore, the spectral location of peak reflection, or peak wavelength value (PWV) can be given by

$$\lambda = n_{\text{eff}}\Lambda \tag{1}$$

where λ is the resonant wavelength, n_{eff} is the effective index, and Λ is the modulation period [5]. The effective index can be considered a weighted average of the refractive indices of the materials in which the standing wave generated at resonance, referred to as the "resonant mode," is supported. The weighting is determined by the fractional electromagnetic intensity in each region

$$n_{\text{eff}}^2 = \frac{\int_{-\infty}^{\infty}\int_{0}^{\Lambda}\varepsilon(x,z)|E(x,z)|^2 dxdz}{\int_{-\infty}^{\infty}\int_{0}^{\Lambda}|E(x,z)|^2 dxdz} \tag{2}$$

where $\varepsilon(x,z)$ and $E(x,z)$ are the two-dimensional spatial distributions of the dielectric permittivity and electric field, respectively. A change in integration bounds due to the modulation period does not modify the effective index because of the normalization. However, the period does influence the electric-field distribution as will be shown later.

The biosensor functions by measuring PWV shifts due to effective index changes resulting from adsorbed biomaterial as given by the differential of (1)

$$\Delta\lambda = \Delta n_{\text{eff}}\Lambda. \tag{3}$$

Any refractive index change of the superstrate media or any dielectric permittivity increase due to adsorption of a surface-bound biomolecular layer will influence the effective index and, consequently, induce a shift in the PWV. Since the effective index is weighted by the normalized resonant electromagnetic intensity at any given point, one must develop a model that describes the field distribution as a function of material and geometric parameters to understand how to optimize a PC biosensor. For surface-based affinity biosensing, sensor performance is directly proportional to the extent of PWV tuning for a given dielectric permittivity variation within the biomolecular detection zone. While the size of the detection zone is defined by the specific sensing application, we consider here only surface-based biomolecular sensing for which we define the detection zone as the volume lying within 25 nm from all exposed surfaces at the top of the device. Motivation for the selection of this detection zone extent is given in the following section. Sensor resolution is inversely related to the spectral width of the resonant reflectance peak since the accuracy in resolving changes in PWV is greatest for a narrow linewidth [9].

The change in effective index can be written as

$$\Delta n_{\text{eff}} = \sqrt{\varepsilon_c + I_D\varepsilon_{D2}} - \sqrt{\varepsilon_c + I_D\varepsilon_{D1}} \tag{4}$$

where the contribution to the effective index has been divided into two components. The fractional dielectric permittivity contribution due to constant regions of the device and environment is given by

$$\varepsilon_C = \frac{\iint_C \varepsilon(x,z)|E(x,z)|^2 dxdz}{\int_{-\infty}^{\infty}\int_{0}^{\Lambda}|E(x,z)|^2 dxdz} \tag{5}$$

where C defines the extent of the constant region. The contribution from the detection zone is given by the product of the permittivity in that region and the resonant mode's field intensity overlap with the biomolecular detection zone

$$I_D = \frac{\iint_D |E(x,z)|^2 dxdz}{\int_{-\infty}^{\infty}\int_{0}^{\Lambda}|E(x,z)|^2 dxdz} \tag{6}$$

where D is the detection zone as defined previously. The quantities ε_{D2} and ε_{D1} are the final and initial dielectric permittivity in the detection zone, respectively. Two-dimensional integrals are sufficient because neither the device nor the resonant fields vary in the y-direction for a one-dimensional grating surface structure. Sensitivity to bulk solution changes of the superstrate can be determined by extending the detection zone out to positive infinity. A similar methodology of using the integrated intensity in the superstrate has been applied to the sensitivity optimization of other evanescent-wave sensors [10].

Equations (3)–(6) reveal three key variables in determining PC biosensor sensitivity. The most obvious is the grating period, Λ. While at first glance a larger Λ yields a larger $\Delta\lambda$, as will be shown later, the period influences the field distribution and so choosing a large Λ does not always lead to optimum performance. The second important property is the effective index of the device without any immobilized substance on the surface. As revealed by (4), a lower refractive index of the device structure (constant regions) yields more effective index tuning for a given index change in the detection zone. Last, and perhaps most importantly, relative device sensitivity can be quantified in part due to the resonant mode's field intensity overlap with the detection zone I_D. That is, the normalized steady-state electric field intensity of the standing wave excited at resonance in the region bounded by the extent of the detection zone plays a major role in determining PC biosensor sensitivity. Maximum sensitivity is achieved for $I_D = 1$, corresponding to the ideal case of perfect overlap of the resonant field and the detection zone.

III. Results

To investigate the relationship between PC biosensor design parameters, the resulting resonant electric field profiles, and the ultimate device performance, we chose several device configurations to study. We begin with a baseline structure that is most often implemented in our laboratory, and then contrast this with several cases, each with only one critical material

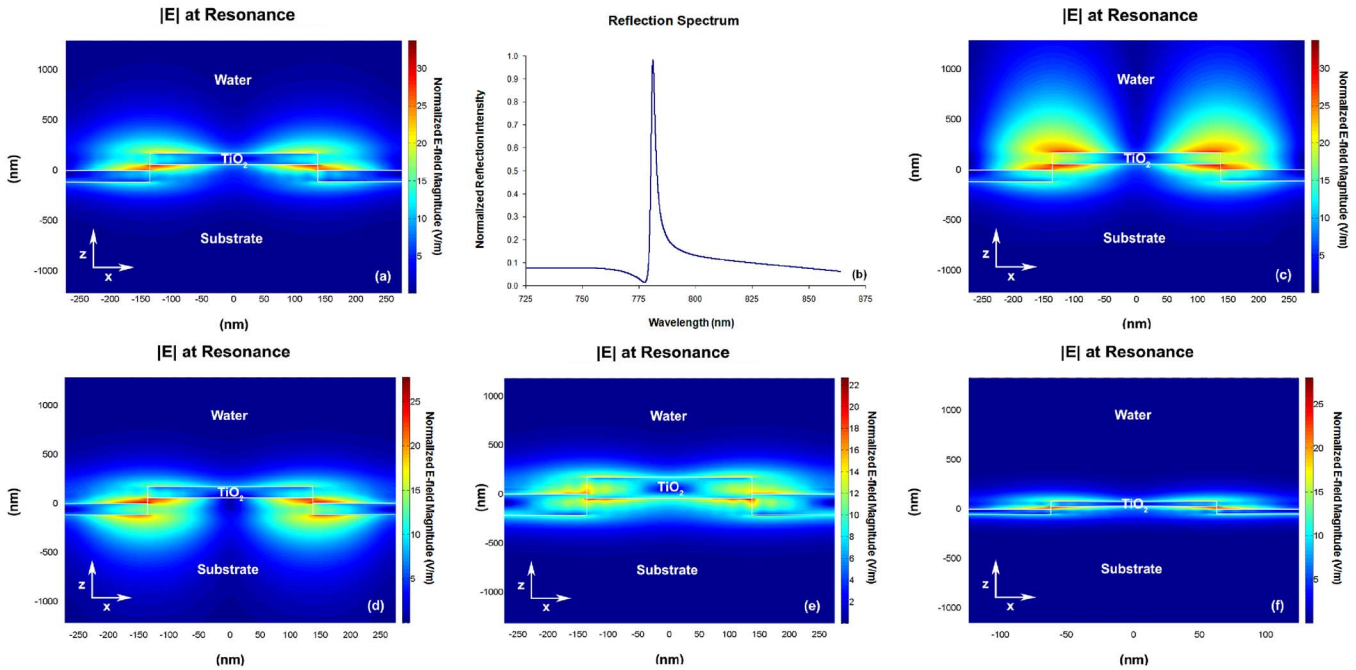

Fig. 2. (a) Electric field profile and (b) reflection spectra for baseline PC biosensor in H_2O superstrate ($n = 1.33$) with $\Lambda = 550$ nm, $t_{\mathrm{TiO2}} = 120$ nm, $n_{\mathrm{TiO2}} = 2.25, t_{\mathrm{step}} = 170$ nm, $n_{\mathrm{sub}} = 1.17$. Field profile for devices deviating from the baseline structure with (c) $n_{\mathrm{TiO2}} = 1.80$, (d) $n_{\mathrm{sub}} = 1.50$, (e) $t_{\mathrm{TiO2}} = 220$ nm, and (f) $\Lambda = 250$ nm, $t_{\mathrm{TiO2}} = 55$ nm, $n_{\mathrm{TiO2}} = 2.67, t_{\mathrm{step}} = 77$ nm. Note modified x axis scale in (f).

or geometrical parameter that has been modified. For each device, we use RCWA to generate a steady-state electric-field cross-section profile at resonance and to calculate resonance location and linewidth. The simulations use TM-polarization, implying the incident and reflected light is polarized with the electric field in the x-direction (perpendicular to the grating lines), the resonantly coupled standing waves have electric field components in the z- and x-directions, and the magnetic field is perpendicular to the plane of incidence in all cases. The TM polarization is selected because it gives a narrower resonant linewidth. Field magnitude rather than intensity plots are given since this provides the most clarity on a linear color scale. Using the electric field profiles and the equations in the previous section, we demonstrate that the precise distribution of these fields is the primary determinant of sensitivity for surface-based label-free biomolecular sensing. While direct RCWA simulations are clearly capable of predicting device sensitivity, the method employed here, as will be seen, provides much greater insight into the origin of sensor performance and is applicable to a wide range of evanescent-wave sensors since the relationship between the field distributions and detection sensitivity holds across all these optical devices. Later, we provide an error analysis to support the validity of using resonant electric fields along with the model in Section II to predict device sensitivity.

To discuss resonant electric field distributions we must define two properties. First is the positioning of the modal axis, or the centerline through the resonant mode along the photonic crystal. The second property is the modal extent, or penetration depth, defining how sharply evanescent the field is about the modal axis. For maximum sensitivity to surface-bound biomolecules, the modal axis should lie just above the device surface and the modal extent should be minimal. In this ideal scenario, the resonant mode would perfectly overlap the active binding region of the device ($I_D = 1$) and the index change in that region would produce a maximal change in the effective index.

A simulated electric field profile, where the magnitudes have been normalized to the incident field, and reflection spectrum are plotted in Fig. 2(a) and (b), respectively, for a common configuration of the PC biosensor with water ($n = 1.33$) as the superstrate. Table I summarizes the spectral characteristics as calculated by direct RCWA simulation and the sensitivity predictions using the model given in Section II. Sensor response to the addition of a biomolecular layer to the detection zone is calculated by the model proposed in Section II. The biomolecules in this study are represented by an $n = 1.40$ material filling the 25-nm-thick detection region. This index is a good approximation to a moderate density organic layer, and the detection zone extent is reasonable for a sensor immobilized with a polymeric coating and detecting large proteins [11]. A superstrate exchange between water ($n = 1.33$) and isopropyl alcohol (IPA, $n = 1.38$) is used to calculate bulk sensitivity with the sensitivity model. The refractive index of IPA provides a reasonable upper limit for most biological assays [12].

To illustrate the effects that physical device properties have on spectral characteristics, steady-state electric field distributions and sensitivity, several cases follow that investigate the consequences of changes in a single device parameter from the baseline structure presented in Fig. 2(a). Field distributions are presented for each case, and the surface sensitivity predictions and spectral properties are tabulated in Table I. TiO_2 is selected as the material system for the high-index coating in order to account for dispersion in the necessary cases.

TABLE I
PC BIOSENSOR SENSITIVITY AND SPECTRAL CHARACTERISTICS FOR SEVERAL DEVICE CONFIGURATIONS

Device Parameters						Direct RCWA Simulation		Model Predictions			
Device #	Λ (nm)	t_{step} (nm)	n_{lo}	t_{hi} (nm)	n_{hi}	PWV (nm)	FWHM (nm)	I_D (%)	SS (nm)	I_∞ (%)	BSC (nm/RIU)
1	550	170	1.17	120	2.25	780.1	2.6	15.7	5.61	57.9	310
2	550	170	1.17	120	1.80	741.3	1.0	9.8	3.69	72.5	394
3	550	170	1.50	120	2.25	854.0	1.0	10.2	3.32	27.1	129
4	550	170	1.17	220	2.25	900.7	3.3	12.3	3.72	35.7	157
5	250	77	1.17	55	2.67	374.1	2.2	30.4	4.64	52.1	117

Λ (period), t_{step} (grating step height), n_{lo} (nanostructured index), t_{hi} (high index coating thickness), n_{hi} (coating index), SS (surface shift), BSC (bulk shift coefficient), RIU (refractive index units).

Fig. 2(c) gives the resonant modal profile for a device using an $n = 1.80$ high-index coating, where this refractive index can be achieved by depositing TiO_2 with an e-beam evaporator. As compared with the baseline device (with $n = 2.25$ TiO_2 film, achievable using a sputter system), this sensor has a greater modal extent and a correspondingly smaller I_D for a 25 nm detection zone. However, it should be noted that I_∞ is larger, as given in Table I, illustrating the need to quantify surface sensitivity and to not rely solely on bulk sensitivity for optical biosensor sensitivity characterization.

An $n = 1.50$ nanostructured surface yields an asymmetric modal extent biased towards the substrate and a modal axis that lies deep within the device, as shown in Fig. 2(d). As compared with the baseline structure, the higher index has the undesirable effect of pulling the mode down out of the test solution and reducing both I_D and I_∞. For this device, we can provide experimental verification of the sensitivity model by comparing theoretical predictions made here with previously presented experimental results. For a photonic crystal sensor with properties nearly identical to that of device #3, we have measured a PWV of 858 nm, bulk shift coefficient (BSC) of 140 nm/refractive index unit (RIU), and surface shift of 2.75 nm [3], [13]. The PWV and BSC are in excellent agreement with the values predicted theoretically here of 854 nm and 129 nm/RIU, respectively. The surface sensitivity assay employs a streptavidin monolayer attached through a linker molecule to a polymeric layer immobilized on the device surface. This functional layer can then be used to bind any biotinylated nucleic acid or protein. Considering the difficulty of accurately measuring the thickness and refractive index of these biomolecular layers, $n = 1.40$, 25 nm simulated coating which yields a 3.32 nm PWV shift is in reasonable agreement with the experiment.

Fig. 2(e) shows the resonant field distribution of a device with a thicker TiO_2 film. The result is reduced sensitivity to index changes in the detection zone and a broadened resonance linewidth.

The electric field distribution of an aggressively scaled device is shown in Fig. 2(f) and exhibits a clear penetration depth reduction. As given in Table I for this device (#5), the operating wavelength is significantly lower than for other devices. We therefore take the dispersion of the TiO_2 coating into account since it varies significantly in the near-ultraviolet. The TiO_2 dispersion is much flatter in the near-infrared, and therefore we approximate the index to be constant at these wavelengths. Fig. 3(a) gives the dependence of I_D on periodicity, attributable to the penetration depth variation, along with the resulting surface sensitivity prediction. I_∞ was also calculated as a function of period, and is plotted in Fig. 3(b). It should be noted that the step height and high-index material thickness are scaled in the same ratio as the period to preserve the aspect ratio. This scaling is common practice for photonic crystals and allows a normalization of the device features relative to the res-

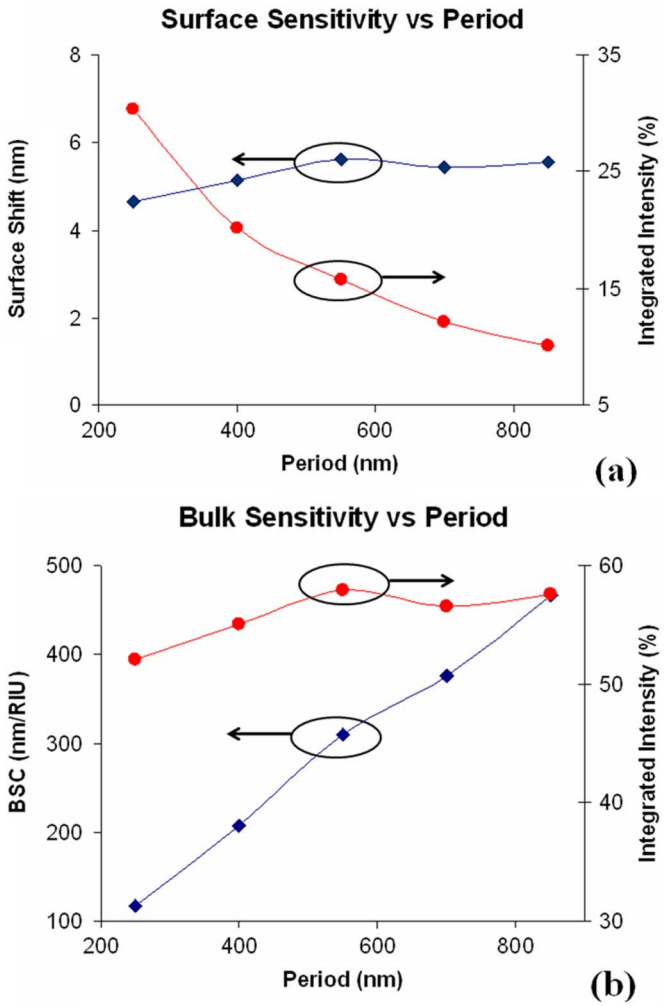

Fig. 3. (a) Surface and (b) bulk sensitivity predictions as a function of modulation periodicity. Other geometrical parameters are scaled with the period to maintain a constant aspect ratio, and TiO_2 refractive index dispersion has been accounted for.

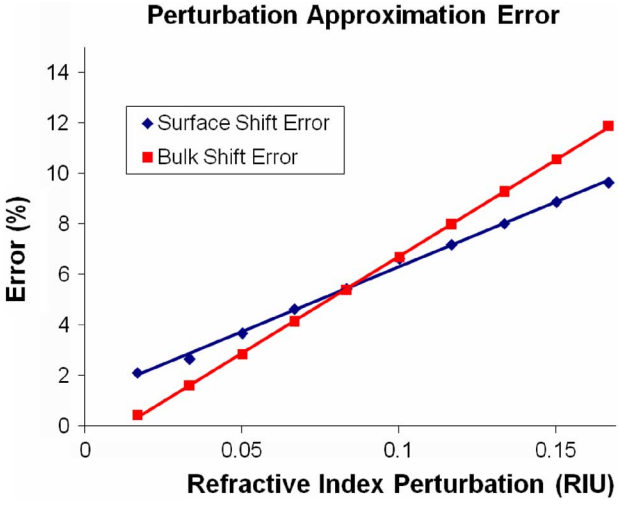

Fig. 4. Error analysis for a 25 nm (surface shift) and infinite (bulk shift) detection zone of varying refractive index computed for device #1. Baseline detection zone contains water ($n = 1.33$).

onant wavelength. For simplicity, this scaling is hereafter implied when we discuss a change in device periodicity. It is also worth mentioning that the TiO_2 dispersion has been accounted for in the data presented in Fig. 3(a) and (b). While penetration depth increases with a larger modulation period, there is little effect on the total integrated intensity in the superstrate since the field is more diffuse throughout the entire simulation domain. The resulting period-dependent bulk sensitivity is shown on the secondary axis in Fig. 3(b). Experimental evidence supporting these phenomena have been demonstrated previously [4].

When permittivity changes are made in the detection zone, the electromagnetic field distribution is altered. However, the model presented assumes the index change is just a small perturbation such that the field remains constant. To affirm that this perturbation approximation is reasonable for the application of biosensing, the error between our sensitivity model and direct RCWA simulation was computed for a range of refractive index changes in the detection zone. Calculations for a 25 nm detection zone as well as one extending to positive infinity were performed for the baseline sensor structure (device #1) to verify model validity for surface and bulk sensitivity, respectively. We define the error as the difference between the PWV shift computed from a constant resonant electric field distribution and that given by direct numerical simulation, normalized to the average of the two. This error is computed at discrete values of refractive index perturbation up to 0.17, corresponding to an index change from water ($n = 1.33$) to a material with $n = 1.50$ in the detection zone (25 nm from the surface for surface shift or extending to positive infinity for bulk shift). Fig. 4 shows that our sensitivity predictions using an $n = 1.40$ 25 nm detection zone and $n = 1.38$ infinite detection zone give less than 5% error for device #1. The error is a function of device parameters, but we compute a worst case error of 7.5% for the bulk sensitivity of device #3. The observed offsets from the origin for the error analyses arise from the meshing approximation generated by the RCWA software.

IV. Discussion

The concepts of "modulation strength" and "index contrast" are the dominant factors in shaping the resonant fields and reflection spectra. The modulation strength is the magnitude of the index differential between the high- and low-refractive index elements of the periodically modulated layer. Index contrast refers to the refractive index differential between the average index of periodically modulated layer and the sub and superstrates. A weaker modulation provides weaker diffraction which results in slower outcoupling to the backward diffracted wave [8]. This increased resonant lifetime yields a higher quality (Q) factor, a measure of the ability of a resonator to store energy. A higher Q defines a cavity with slower energy leakage or equivalently a longer resonant lifetime, and consequently a narrow linewidth in the frequency domain. In the limit, zero modulation gives zero linewidth, as would be expected since this returns us to the case of a waveguide supporting real propagating modes.

For total internal reflection at an interface between two dielectrics, the magnitude of the transmitted electric field into the lower n material is proportional to $e^{-\alpha z}$ where

$$\alpha = \omega\sqrt{\mu_0 n_1^2 \sin^2\theta_i - \mu_0 n_2^2} \tag{7}$$

where ω is the frequency of interest, θ_i is the incident angle with respect to the normal, μ_0 is the dielectric permeability for both nonmagnetic media, and n_1 and n_2 are the indices of the high- and low-refractive index media, respectively [14]. It is clear that a higher index contrast between the periodically modulated surface structure and the superstrate yields less modal extent. Therefore, a larger index contrast gives increased effective index tuning due to the stronger modal overlap with the detection zone. However, it should be noted that this is strongly dependent upon the selected detection zone extent and corresponding application. A further consequence of increased n contrast is a wider resonant linewidth.

The above descriptions can aid in explaining the results of the device illustrated in Fig. 2(c). The larger modal extent is due to the reduced average n of the periodically modulated layer. Furthermore, decreasing the coating index reduces the modulation strength as well as the index contrast, both of which contribute to a significantly narrowed resonant linewidth.

To help tailor the photonic crystal to function optimally as an optical biosensor, the sub and superstrate indices can be adjusted such that the modal axis is situated close to the device surface and the modal extent is asymmetric. By lowering the substrate index, we reduce the modal extent in that region and push the modal axis up towards the device surface since the mode will tend towards regions of highest n. Comparison of Fig. 2(a) and (d), which differ only in their substrate refractive index, demonstrate precisely this behavior. The reduced substrate index of the device simulated in Fig. 2(a) leads to increased modal overlap in the binding region, and consequently larger changes to the effective index upon molecular binding. The larger nanopatterned material n of the device presented in Fig. 2(d) results in a narrowed linewidth by the same arguments presented for the above case of a lower n_{TiO2}. While significantly changing the refractive index of the test media would provide another avenue for

device optimization, doing so is impractical for biological assays and thus not addressed here. The data presented here show that increasing device sensitivity requires extremes in refractive indices, as has been shown previously for guided-wave evanescent sensors [15]. Low index materials that can be readily processed are currently limited to ~ 1.15, while the highest index low-loss material that is transparent in the near-ultraviolet, visible and near-infrared and can be deposited at low temperature for compatibility with plastic substrates is sputtered TiO_2 with $n = 2.25$ at 800 nm. Relaxing the temperature criteria and restricting use to visible wavelengths and longer would enable the use of CVD SiC with $n = 2.5$ at ~ 800 nm. Many other high index materials such as Si_3N_4, Ta_2O_5, and HfO_2 can be used depending upon requirements for operating wavelength, manufacturability, and surface chemistry.

Optimization of the thickness of the high-index layer is also crucial. A thinner layer causes more of the resonant mode to exist in the superstrate, and in effect brings the detection zone closer to the modal axis. On the other hand, the thicker coating yields a desirably higher average n of the periodically modulated layer and more tightly confined resonant fields. Both effects are apparent in Fig. 2(e), which gives the resonant field distribution for a device with a thicker high-index coating. The data in Table I reveal the benefit of tighter modal confinement is overcome by reduced overlap with the liquid media. It is important to note that a minimum thickness is necessary to support a resonance with 100% reflection efficiency. This critical thickness varies with the other properties discussed above and corresponds to a cutoff condition.

The final parameter we consider for optimization is the photonic crystal's modulation period. Since the biosensor functions by PWV shifts due to effective index changes, as given by (3), a larger grating period gives improved sensitivity for a given effective index change. However, the periodicity strongly determines the PWV, as given by (1) and (7) shows that a lower resonant frequency, or equivalently a larger PWV, yields an increased modal extent. The variation of modal extent with modulation periodicity is obvious when comparing Fig. 2(a) and (f) for which the periods are 550 and 250 nm, respectively. The resulting surface sensitivity as a function of period plotted in Fig. 3(a) reveals that these two effects nearly offset one another for the 25 nm detection zone applied in this study. Fig. 3(b) demonstrates there is improved sensitivity as the detection zone is extended towards infinity. The specific sensing application must therefore be carefully considered when selecting the optimal periodicity of a PC biosensor. Furthermore, practical limitations should be considered when selecting the PC period and resulting PWV as very small features require high fabrication costs while long wavelength resonances mandate expensive detection instrumentation.

The typical practice of quoting a bulk sensitivity figure of merit for optical biosensors does not provide an accurate picture of how the device will perform in the context of surface-based biomolecular detection. Generally, the "surface" sensitivity (sensitivity to changes of dielectric permittivity within the detection zone) is correlated with the bulk sensitivity, but this is not always the case. Resonant fields that do not overlap the binding region are not useful for biosensing, whether the energy is situated within the device or out in the bulk media away from the sensor surface. In fact, modal overlap in the test media outside the detection zone is detrimental because fluctuations of the bulk solution refractive index can be a significant source of noise for optical biosensing. Therefore, although Fig. 3(a) shows only a marginal surface sensitivity improvement at shorter periods, the reduction in bulk sensitivity established by Fig. 3(b) should not be overlooked.

The theory and results presented here demonstrate the complex interplay between the many parameters on PC biosensor performance. The modal overlap in the detection zone and the modulation periodicity are shown to strongly influence sensitivity. A careful comparison of devices 2 and 3 from Table I reveals that surface sensitivity (for sensors with equal modulation periods) is not solely a function of I_D, as should be expected from (4). Since device 2 has much of its resonant intensity situated in a low-index medium $(n = 1.33)$, while for device 3, it is in a moderate-index medium $(n = 1.50)$, effective index tuning is greater for the former given a comparable I_D for both sensors. Maximum modal overlap in the detection zone and a minimum effective index are, therefore, ideal for optimizing PC biosensor performance.

A cursory inspection of the field profiles presented in Fig. 2 reveals higher field magnitudes in the lower refractive index materials and a discontinuous distribution along the z axis. The boundary condition stipulating continuity for the electric displacement component normal to the boundary is responsible for this effect. Discontinuities are not readily apparent along the x axis because the magnitude of E_x at resonance is much smaller than that of E_z. The incident and reflected plane waves, polarized with the electric field along the x-direction, do not contribute to the effective index. It is fortuitous that the device is operated with TM-polarized incident light, as this significantly reduces the integrated electric field intensity lying inside the device. TE-polarized incident light would yield maxima in the high-index regions and would greatly reduce I_D.

It is noteworthy that absolute electric field magnitudes play no role in determining label-free biosensor sensitivity. However, they do affect resolution because the field magnitude is correlated to the resonance Q and linewidth, where higher fields are present for larger Q and correspondingly narrower linewidths. While improved biosensor resolution performance mandates extremely narrow resonances, this is difficult to achieve in practice due to the increased stringency for low-loss materials supporting high field magnitudes and the need for highly collimated incident light. It is therefore more practical to design a PC biosensor based solely on surface sensitivity as the theoretical resonances become very narrow.

The theory and data presented in this paper have focused on the sensitivity of PC biosensors to refractive index changes, but not on the ultimate application of detecting biomolecular interactions. If the resolution of the detection setup is known, this information along with the computed sensitivity can be used to predict the minimal refractive index discrimination. However, the limit of detection for a specific molecular species cannot be determined solely with the model presented here, as the complex surface binding kinetics of the test solution must also be known.

V. Conclusion

In conclusion, we have presented for the first time a theoretical basis for PC biosensor sensitivity based on the understanding of near-field distributions in such resonators. Electric field profiles and reflection spectra calculated using RCWA for several device configurations help to clearly validate this theory. The model and data support previous experimental reports of improved sensor performance through the incorporation of a low-index material and the scaling down of device dimensions. We believe this work's results and the supporting commentary are invaluable for the optimization not only of PC biosensors, but of any optical sensor that relies on the interaction of electromagnetic near-fields to monitor the changes in its immediate vicinity. Furthermore, the improved ability to carefully tune resonant near-fields may find application in a range of other PC devices such as those employed for fluorescence and nonlinear enhancement.

References

[1] B. T. Cunningham *et al.*, "Label-free assays on the BIND system," *J. Biomol. Screening*, vol. 9, pp. 481–490, 2004.

[2] P. Li, B. Lin, J. Gerstenmaier, and B. T. Cunningham, "A new method for label-free imaging of biomolecular interactions," *Sens. Actuators B*, vol. 99, pp. 6–13, 2004.

[3] I. D. Block, L. L. Chan, and B. T. Cunningham, "Photonic crystal optical biosensor incorporating structured low-index porous dielectric," *Sens. Actuators B*, vol. 120, pp. 187–193, 2006.

[4] N. Ganesh, I. D. Block, and B. T. Cunningham, "Near ultraviolet-wavelength photonic-crystal biosensor with enhanced surface-to-bulk sensitivity ratio," *App. Phys. Lett.*, vol. 89, pp. 23901–23904, 2006.

[5] R. Magnusson *et al.*, "Photonic devices enabled by waveguide-mode resonance effects in periodically modulated films," in *Proc. SPIE Nano- and Micro-Optics Inf. Syst.*, 2003, vol. 5225, pp. 20–34.

[6] A. Hessel and A. A. Oliner, "A new theory of wood's anomalies on optical gratings," *Appl. Opt.*, vol. 4, pp. 1275–1297, 1965.

[7] S. S. Wang and R. Magnusson, "Theory and applications of guided-mode resonance filters," *Appl. Opt.*, vol. 32, pp. 2606–2613, 1993.

[8] D. Rosenblatt, A. Sharon, and A. A. Friesem, "Resonant grating waveguide structures," *IEEE J. Quantum Elect.*, vol. 33, pp. 2038–2059, 1997.

[9] W. C. Karl and H. H. Pien, "High-resolution biosensor spectral peak shift estimation," *IEEE Trans. Signal Processing*, vol. 53, pp. 4631–4639, 2005.

[10] O. Wolfbeis, *Fiber Optic Chemical Sensors and Biosensors*. Boca Raton, FL: CRC Press, 1991, pp. 111–192.

[11] J. Voros, "The density and refractive index of adsorbing protein layers," *Biophys. J.*, vol. 87, pp. 553–561, 2004.

[12] N. E. Good, G. D. Winget, W. Winter, T. N. Connolly, S. Izawa, and R. M. M. Singh, "Hydrogen ion buffers for biological research," *Biochemistry*, vol. 5, p. 467, 1966.

[13] W. Zhang, N. Ganesh, I. D. Block, and B. T. Cunningham, "High sensitivity photonic crystal biosensor incorporating nanorod structures for enhanced surface area," *Sensors. and Actuators B*, Sep. 2007, In Press.

[14] C. Balanis, *Advanced Engineering Electromagnetics*. New York: Wiley, 1989, p. 200.

[15] O. Parriaux *et al.*, "Evanescent wave sensor of sensitivity larger than a free space wave," *Optical and Quantum Elect.*, vol. 32, pp. 909–921, 2000.

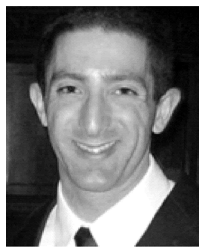

Ian D. Block received the B.S. degree in electrical and computer engineering from Cornell University, Ithaca, NY, in 2004, and the M.S. degree in electrical engineering from the University of Illinois at Urbana–Champaign, Urbana, in 2005. He is currently working towards the Ph.D. under the direction of Dr. Brian Cunningham at the University of Illinois.

The focus of his research is the design and characterization of optical biosensors.

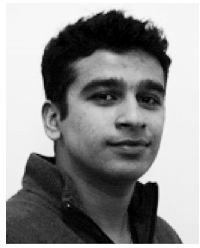

Nikhil Ganesh received the B.E. degree in polymer sciences and chemical technology from the Delhi College of Engineering, New Delhi, in 2004. He is currently working towards the Ph.D. degree in the Department of Materials Science and Engineering, University of Illinois at Urbana–Champaign, Urbana.

His research interests include nanophotonics and biosensors.

Meng Lu received the B.S. degree in electrical engineering from the University of Science and Technology of China, Hefei, in 2002 and the M.S. degree in electrical engineering from the University of Illinois at Urbana–Champaign, Urbana, in 2004. He is currently working towards the Ph.D. degree at the University of Illinois at Urbana–Champaign.

His research focuses on the development and application of optical resonators.

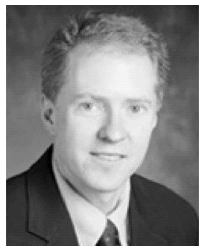

Brian T. Cunningham (M'02–SM'07) received the B.S., M.S., and Ph.D. degrees in electrical and computer engineering from the University of Illinois at Urbana–Champaign, Urban, in 1986, 1987, and 1990, respectively. His thesis research was in the field of optoelectronics and compound semiconductor material science, where he contributed to the development of crystal growth techniques that are now widely used for manufacturing solid-state lasers, and high frequency amplifiers for wireless communication.

He is currently the Director of the Nano Sensors Group in the Electrical and Computer Engineering Department, University of Illinois at Urbana–Champaign. His group focuses on the development of photonic crystal-based transducers, plastic-based fabrication methods, and novel instrumentation approaches for label-free biodetection. He is a founder and the Chief Technical Officer of SRU Biosystems (Woburn, MA), a life science tools company that provides high sensitivity plastic-based optical biosensors, instrumentation, and software to the pharmaceutical, academic research, genomics, and proteomics communities. Prior to founding SRU Biosystems in June 2000, he was the Manager of Biomedical Technology at Draper Laboratory, Cambridge, MA, where he directed R&D projects aimed at utilizing defense-related technical capabilities for medical applications. In addition, he served as Group Leader for MEMS Sensors at Draper Laboratory, where he directed a group performing applied research on microfabricated inertial sensors, acoustic sensors, optical switches, microfluidics, tissue engineering, and biosensors. Concurrently, he was an Associate Director of the Center for Innovative Minimally Invasive Therapy (CIMIT), a Boston-area medical technology consortium, where he led the Advanced Technology Team on microsensors. Before working at Draper Laboratory, he spent five years at the Raytheon Electronic Systems Division developing advanced infrared imaging array technology for defense and commercial applications.